Robertson, A.H.F., Emeis, K.-C., Richter, C., and Camerlenghi, A. (Eds.), 1998
Proceedings of the Ocean Drilling Program, Scientific Results, Vol. 160

20. SEDIMENTARY SULFUR AND IRON CHEMISTRY IN RELATION TO THE FORMATION OF EASTERN MEDITERRANEAN SAPROPELS[1]

Hilde F. Passier[2] and Gert J. de Lange[2]

ABSTRACT

Detailed analyses of total sulfur, pyritic sulfur, humic sulfur, NaCl-extractable sulfur, elemental sulfur, acid-volatile sulfide, and organic polysulfide in and around the most recent Sapropel S1 (maximum C_{org} = 2.3%) and two other sapropels recovered during Ocean Drilling Program Leg 160 (maximum C_{org} = 7.4% and 23.5%), show that the main sulfur species in and immediately below each sapropel is pyrite. Directly above each sapropel sulfur is rarely present in the solid phase, but occurs as pore-water sulfate (SO_4^{2-}). Microbial SO_4^{2-} reduction took place in the sapropels during sapropel formation. Addition of reactive iron to sapropel layers occurred via upward diffusion of Fe^{2+} from underlying sediments and/or through water-column iron sulfide precipitation. All reactive iron that was available in the sediments was used for pyrite formation. As a result, diffusion of sulfide out of the sapropels and sulfidization of the sediments underlying each sapropel have occurred. Only in the most C_{org}-rich sapropel did large-scale uptake of reduced sulfur by organic molecules occur, and SO_4^{2-} reduction probably still continues.

INTRODUCTION

Bacterial sulfate reduction is a common feature in organic-rich sediments in the marine environment (e.g., Canfield, 1989; Mossmann et al.,1991; Calvert and Karlin, 1991). It is part of the complex redox system related to the oxidation of organic matter (Froelich et al., 1979). The sulfur enrichments in the recurrent organic-rich layers (sapropels) in the Eastern Mediterranean prove that these have been subject to bacterial SO_4^{2-} reduction (Van Os et al., 1991; Pruysers et al., 1993; Passier et al., 1996).

The sequence of alternating organic-rich and organic-poor layers in the sedimentary record of the Eastern Mediterranean provides a unique setting to study the different paleoenvironmental and diagenetic signals. During sapropel formation, bacterial sulfate reduction dominated the anoxic sediment at the sediment/water interface, whereas the organic matter oxidation in underlying sediments was dominated by reduction of iron (hydr)oxides. The classic downward succession of oxic, suboxic, and anoxic sediment (Froelich et al., 1979) does not apply to this dynamic system. Relicts of the different redox regimes can be found in the sediment column. For example, enrichments in reduced sulfur species indicate episodes of sulfate reduction, and iron (hydr)oxide-enriched layers indicate boundaries of oxic and suboxic sediments (e.g., Van Santvoort et al., 1996).

A striking feature is that most of the diagenetic alteration of Eastern Mediterranean sediments takes place during and relatively shortly after their formation. Most diagenetic features inferred from sulfur and iron chemistry of Pleistocene sapropels recovered by gravity-coring techniques are also present in the sediments in and around the most recent Holocene Sapropel S1 (5–9 k.y.) (Higgs et al., 1994; Passier et al., 1996; Van Santvoort et al., 1996). In this study we compare the sulfur and iron chemistry of two sapropels of Pliocene age recovered during Ocean Drilling Program (ODP) Leg 160 with the most recent Sapropel S1, to gain insight into the factors that determine the diagenetic history of these sapropels.

MATERIALS AND METHODS

Three sapropels were studied. Sapropel S1 in box-core UM26 (33°23.6′N, 25°0.9′E, water depth 2160 m) was recovered 200 km south of Crete during the 1994 Palaeoflux cruise of *Urania*. The sapropel, at about 0.24 m below seafloor (mbsf), is 4 cm thick. Light gray sediments lie beneath the sapropel; orange-brown sediments lie above it. Part of UM26 was sampled at a resolution of 0.5–1 cm aboard ship inside an N_2-filled glovebox and stored under N_2 in airtight containers at 4°C.

Two sapropels, recovered during Leg 160, were sampled in detail directly after core splitting aboard *JOIDES Resolution*. One of the Leg 160 sapropels was recovered in Section 160-969E-6H-6. Site 969E (33°50.5′N, 24°53.0′E, water depth 2201 m) is located on the Mediterranean Ridge, close to the UM26 site. Hole 969E contains 80 sapropel beds of early Pliocene to Holocene age. The sampled interval contains a 12-cm-thick black sapropel at 50.7 mbsf (at 27 cm in the section), surrounded by light gray sediments. This sapropel belongs to a group of black sapropels of middle Pliocene age with high organic carbon contents (up to 30%) in a gray interval. The dark sapropel has a fine bedding-parallel parting, which may be the result of primary lamination (Emeis, Robertson, Richter, et al., 1996). The other Leg 160 sapropel originates from Section 160-967C-6H-2. Site 967C (34°4.3′N, 32°43.5′E, water depth 2553 m) is located on a small ridge near the foot of the northern slope of the Eratosthenes Seamount, about 70 km south of Cyprus. At this site, 80 sapropels of early Pliocene to Holocene age were recovered. The sampled interval contains a 14-cm-thick sapropel at 49.3 mbsf (at 30 cm in the section). The sapropel is brownish black and surrounded by gray sediments. It is of late Pliocene age and appears bioturbated. Ten samples 1.5 cm thick were taken over intervals of 50 and 30 cm in sections 967C-6H-2 and 969E-6H-6, respectively. The samples were stored under N_2 in airtight containers at 4°C.

Subsamples were dried at 40°C (UM26) or freeze-dried (Leg 160) and ground in an agate mortar before dissolution in an $HClO_4$–HNO_3–HF acid mixture. The dried residue was dissolved in 1M HCl for analysis of total sulfur (S_{tot}), total iron (Fe_{tot}) and total aluminum (Al_{tot}) with a Perkin Elmer OPTIMA 3000 inductively coupled plasma atomic emission spectrometer (ICP-AES). Organic carbon contents were determined with a Fisons Instruments NA-1500 NCS ana-

[1]Robertson, A.H.F., Emeis, K.-C., Richter, C., and Camerlenghi, A. (Eds.), 1998. *Proc. ODP, Sci. Results*, 160: College Station, TX (Ocean Drilling Program).

[2]Department of Geochemistry, Institute of Earth Sciences, Utrecht University, PO Box 80.021, 3508 TA Utrecht, The Netherlands. hpassier@earth.ruu.nl

lyzer after removal of carbonate in 1M HCl. S_{tot}, Fe_{tot}, Al_{tot}, and C_{org} measurements were performed according to standard laboratory procedures and have standard deviations <5%. International and in-house standards were used to check the procedures.

Dried subsamples were extracted with acetone for several hours to remove elemental sulfur (including elemental sulfur formed during drying from acid-volatile sulfide [AVS] and organic polysulfides, and elemental sulfur originally present) before pyrite extraction. Pyrite sulfur (S_{pyr}) was extracted with the Cr(II) reduction method (Zhabina and Volkov, 1978; Canfield et al., 1986; Cutter and Oatts, 1987; Henneke, 1993; Henneke et al., 1997). AVS (consisting of iron monosulfides) was extracted from wet subsamples in 6M HCl under an N_2 or Ar atmosphere. H_2S that evolved in the pyrite and AVS extractions was stripped from reaction solutions with N_2 or Ar and trapped in 1M NaOH. The NaOH solution was analyzed for HS^- by square-wave voltammetry (SWV) with a Princeton Applied Research Model 384B-4 polarographic analyzer system equipped with a Model 303A static mercury drop electrode (SMDE).

A sequential extraction procedure (Henneke, 1993; Henneke et al., 1997, based on Francois, 1987, and Ferdelman et al., 1991) was applied to wet subsamples under an N_2 atmosphere. First, easily removable sulfur (S_{NaCl}, mostly porewater S) was extracted by 0.5 M NaCl. Then, elemental sulfur (S_{elem}; including low-molecular-weight organic sulfur) was extracted by methanol:toluene (3:1); pure methanol was used for UM26. Subsequently, organic polysulfides (S_{orgpol}) were broken down to elemental sulfur in 1M HCl and extracted by methanol:toluene (3:1); pure methanol was used for UM26. After rinsing the sample with demineralized water, humic sulfur (S_{NaOH}) was extracted by 0.5 M NaOH. Elemental-sulfur-containing-extracts were evaporated and SO_3^{2-} was added to convert elemental sulfur to $S_2O_3^{2-}$, which was determined by (cathodic stripping [CS]) SWV. NaCl and NaOH extracts were analyzed for major elements by ICP-AES.

The residue of the sequential extraction was dissolved in an $HClO_4$–HNO_3–HF acid mixture, dried, and dissolved in 1 M HCl for analysis of sulfur by ICP-AES. The residual phases of the sequential extraction are pyrite and nonextractable organic sulfur.

The reproducibility of sulfur species analyses appeared dependent of the content and the amount of material available for measurement. Reproducibility was poor for measurements of S_{orgpol} in samples from Leg 160 sapropels below 1–2 µmol/g dry, of S_{elem} in Leg 160 samples below 0.1–0.2 µmol/g dry, and of AVS in all samples below 0.01 µmol/g dry. These poorly reproducible data showed relative deviations from the mean of 40%–145%. All other measurements were satisfactorily reproducible. The average relative deviations from the mean in duplicate measurements were 10% for pyrite and AVS, 8% for residual sulfur, 12% for S_{elem} and S_{orgpol}, 5% for S_{NaCl}, and 9% for S_{NaOH}.

Reactive iron was extracted from wet subsamples in dithionite (acetate/citrate buffer, pH = 4.8, 4 hr, 60°C) under an N_2 atmosphere following the procedure of Kostka and Luther (1994). Dithionite is thought to extract amorphous iron (hydr)oxides, crystalline iron (hydr)oxides, and AVS. The iron concentration in the dithionite extracts was measured by ICP-AES and spectrophotometrically (Köster, 1979). The average relative deviation from the mean in duplicate measurements of reactive iron was 10%.

The water contents of the samples were determined by differences in weight before and after drying.

RESULTS

Sapropel samples are relatively rich in sulfur and organic carbon (C_{org}) (Fig. 1; Table 1). The predominant sulfur phase in and below each sapropel is S_{pyr} (Fig.1; Table 1). Above sapropels, however, humic sulfur (S_{NaOH}) and S_{NaCl} are the most important sulfur species (Fig. 1, Table 1). The C_{org} contents of the three sapropels differ significantly: the maxima are 2.3, 7.4, and 23.5 wt% for the sapropel samples from Core UM26, and Sections 967C-6H-2, 30 cm, and 969E-6H-6, 27 cm, respectively. The C_{org} content in nonsapropel samples ranges from 0.1 to 0.6 wt% (Fig. 1; Table 1).

S_{NaCl} is fairly constant in samples from Core UM26 and Section 967C-6H-2, 30 cm, and both cores have similar contents. At the bottom of the sapropel in Section 969E-6H-6, 27 cm, however, the S_{NaCl} is 1 order of magnitude higher (Fig. 1; Table 1).

S_{NaOH} is enriched in all three sapropel layers: the maximum contents are 27, 71, and 121 µmol/g dry for sapropel samples UM26, 967C-6H-2, 30 cm, and 969E-6H-6, 27 cm, respectively (Fig. 1; Table 1). S_{NaOH} below the sapropels is slightly higher than above them. In the NaOH extraction a small amount of pyrite may be co-extracted. Deduced from the iron contents of the humic extract, less than 15% of the sulfur extracted by NaOH in pyrite-rich samples may be pyritic sulfur. This is a maximum percentage, because iron phases other than pyrite dissolve in 0.5 M NaOH as well.

The main residual sulfur phases of the sequential extraction are pyrite and nonextractable organic sulfur. In most samples, the amount of residual sulfur of the sequential extraction is comparable to or slightly smaller than the amount of pyritic sulfur. Minor losses may have occurred during the sequential extraction procedure. In 969E-6H-6, 27 cm, however, the amount of residual sulfur is greater than the amount of pyritic sulfur (Fig. 2). Accordingly, nonextractable organic sulfur may be present.

S_{elem} content is less than 0.06 µmol/g dry in Core UM26, and there is no apparent trend with depth. In contrast, S_{elem} is enriched to 0.6 µmol/g dry in 967C-6H-2, 30 cm, and to 23 µmol/g dry in 969E-6H-6, 27 cm, and it correlates positively with the C_{org} content (Fig. 1; Table 1). S_{orgpol} content is less than 2 µmol/g dry in 967C-6H-2, 30 cm, and Core UM26, and there is no noticeable trend with depth. In 969E-6H-6, 27 cm, though, the S_{orgpol} content correlates positively with the C_{org} content and is 4.3 µmol/g dry at maximum (Fig. 1; Table 1). AVS contents are low: 0 to 0.4 µmol/g dry in Core UM26, 0.03 to 0.9 µmol/g dry in Section 967C-6H-2, 30 cm, and 0.02 to 0.7 µmol/g dry in Section 969E-6H-6, 27 cm (Fig. 1; Table 1). AVS contents in samples from sapropel S1 measured directly aboard after sampling inside an N_2-filled glovebox were in the same range.

Because the AVS contents are relatively small, all dithionite-extractable iron may be considered to represent iron (hydr)oxides. Iron (hydr)oxides (Fe_{dith}; Fig. 3; Table 1) are relatively enriched above the sapropels in Section 967C-6H-2, 30 cm, and in Core UM26, and at the base of the sapropel in Section 969E-6H-6, 27 cm.

Independently determined total sulfur contents (S_{tot}; Fig. 1; Table 1) compare well with the sum of all sulfur species recovered in the sequential extraction (Table 2).

DISCUSSION

Sulfur Species

NaCl-Extractable Sulfur

In view of the good correlation with the water content (Fig. 4), the NaCl-extracted sulfur is largely attributable to porewater SO_4^{2-}. The average porewater SO_4^{2-} concentration, calculated from the water contents and S_{NaCl}, is 34 mM (standard deviation 4%), without any trend with depth. This is close to the concentration of SO_4^{2-} in Mediterranean seawater (32 mM). The water contents of the Leg 160 samples could not be accurately determined, as the samples had been subject to evaporation aboard ship. Compared to the S_{NaCl} values of Core UM26 and to the SO_4^{2-} porewater concentration measured aboard (Sites 969 and 967, at 50 mbsf: 32 mM), S_{NaCl} in Section 967C-6H-2, 30 cm, can be entirely attributed to porewater SO_4^{2-}. At the bottom of the sapropel in Section 969E-6H-6, 27 cm, however, the amount of S_{NaCl} is excessive compared with porewater SO_4^{2-}. A tentative con-

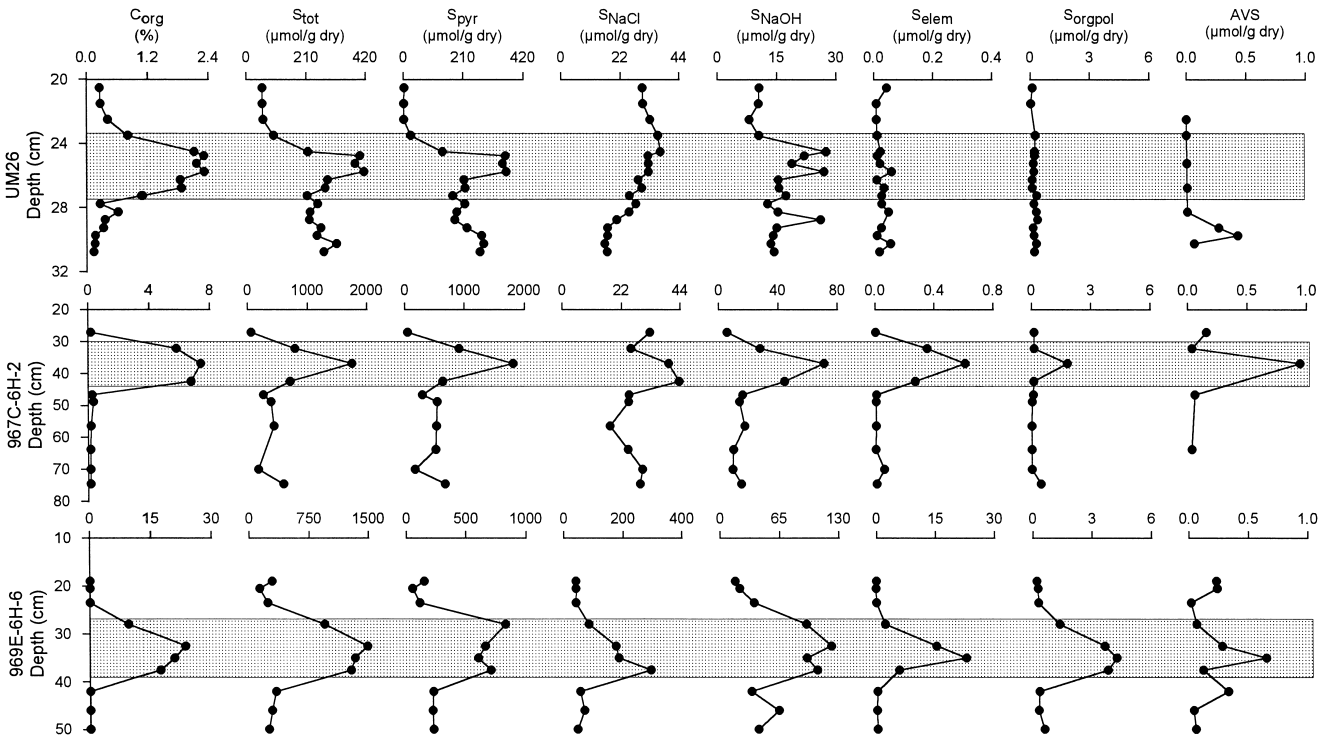

Figure 1. Content vs. depth profiles of C_{org}, S_{tot} (total sulfur contents of the samples), S_{pyr} (pyritic sulfur, determined by Cr(II) reduction), S_{NaCl} (NaCl-extractable sulfur), S_{NaOH} (NaOH-extractable, humic sulfur), S_{elem} (elemental sulfur including low-molecular-weight organic sulfur), S_{orgpol} (organic polysulfides), and AVS (acid-volatile sulfide, extracted with 6M HCl) in samples from Core UM26, and intervals 967C-6H-2, 26–75 cm, and 969E-6H-6, 19–50 cm. The shaded bands indicate the position of the sapropels.

Table 1. Range of contents of C_{org}, S_{tot}, S_{pyr}, S_{NaCl}, S_{NaOH}, S_{elem}, S_{orgpol}, AVS, and Fe_{dith}.

Samples	C_{org} (wt%)	S_{tot} (µmol/g dry)	S_{pyr} (µmol/g dry)	S_{NaCl} (µmol/g dry)	S_{NaOH} (µmol/g dry)	S_{elem} (µmol/g dry)	S_{orgpol} (µmol/g dry)	AVS (µmol/g dry)	Fe_{dith} (µmol/g dry)
S1, UM26									
Above	0.3-0.4	56-58	0.3-2.0	30-33	8-11	0.01-0.04	0.00-0.11	0.00	70-99
Within	0.8-2.3	95-415	25-360	25-37	10-27	0.01-0.06	0.09-0.32	0.00-0.01	5-93
Below	0.1-0.6	219-317	180-281	16-28	13-26	0.01-0.06	0.13-0.37	0.01-0.43	3-9
160-967C-6H-2, 30 cm									
Above	0.2	54	44	33	6	0.00	0.14	0.16	126
Within	5.8-7.4	703-1749	632-1815	25-44	28-71	0.27-0.61	0.12-1.82	0.04-0.95	58-78
Below	0.2-0.4	169-589	158-665	18-30	9-17	0.00-0.06	0.01-0.46	0.03-0.06	48-67
160-969E-6H-6, 27 cm									
Above	0.1	130-287	51-147	41	16-37	0.00	0.20-0.28	0.02-0.24	6-7
Within	9.6-23.5	938-1486	600-828	83-294	94-121	2.2-22.8	1.36-4.25	0.06-0.65	27-225
Below	0.1	240-329	215-222	44-67	34-64	0.00-0.11	0.29-0.56	0.04-0.33	8-10

Notes: S_{tot} = total sulfur, S_{pyr} = pyritic sulfur, S_{NaCl} = NaCl-extractable sulfur, S_{NaOH} = NaOH-extractable, humic sulfur, S_{elem} = elemental sulfur, including low-molecular-weight organic sulfur, S_{orgpol} = organic polysulfides, AVS = acid-volatile sulfides, and Fe_{dith} = dithionite extractable iron. The values are grouped according to position relative to sapropel.

clusion (see following discussion) from the 1:1 ratio of Ca and S in the NaCl extracts of Section 969E-6H-6, 27 cm, (Fig. 5) is that this enrichment is probably gypsum ($CaSO_4 \cdot 2H_2O$). There is no correlation with sulfur for the elements Ba, K, Sr, and Fe in the NaCl extracts of Section 969E-6H-6, 27 cm.

Organic Polysulfide Sulfur, Elemental Sulfur, and AVS

Insignificant amounts of AVS, S_{elem} and S_{orgpol}, all of which are possible intermediates in pyrite formation (e.g., Luther and Church, 1992) were found in Core UM26 (Fig. 1). Because long-term accumulation of intermediate species is not likely in these marine sediments, the intermediates are indicators for active SO_4^{2-} reduction. This indicates that no substantial SO_4^{2-} reduction and no pyrite formation presently occur in these sediments. The contents of S_{orgpol} and S_{elem} in Section 969E-6H-6, 27 cm, and S_{elem} in Section 967C-6H-2, 30 cm, correlate with the C_{org} contents (Fig. 1). These enrichments have formed at places where the sulfide concentrations were high, resulting from in situ SO_4^{2-} reduction, within the sapropel. Elemental sulfur forms from partial oxidation of sulfide, and organic polysulfides form by incorporation of sulfide in organic matter. The contents of AVS, elemental sulfur, and organic polysulfide sulfur are in general higher in Section 969E-6H-6, 27 cm, and 967C-6H-2, 30 cm, than they are in Core UM26, albeit they are still at relatively low levels. This indicates that relatively more SO_4^{2-} reduction occurs, although still at a low level, at present in the older sapropels than in the

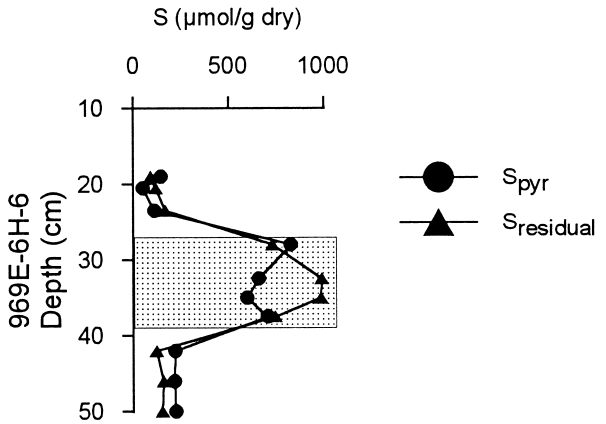

Figure 2. Content vs. depth profiles of S_{pyr} (pyritic sulfur determined by Cr(II) reduction) and $S_{residual}$ (residual amount of sulfur of the sequential extraction) in interval 969E-6H-6, 19–50 cm. The difference between the two species indicates the presence of nonextractable organic sulfur. The shaded band indicates the position of the sapropel.

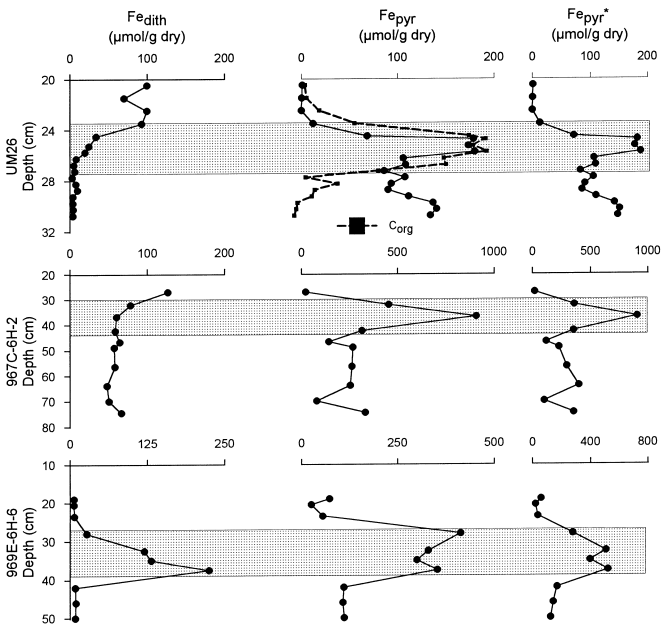

Figure 3. Content vs. depth profiles of Fe_{dith} (dithionite-extractable iron), Fe_{pyr} ($0.5 \times S_{pyr}$, with S_{pyr} determined by Cr(II) reduction), and Fe_{pyr}* (average $Al_{tot} \times Fe_{pyr}/Al_{tot}$ [normalization to aluminum]) in Core UM26, and intervals 967C-6H-2, 26–75 cm, and 969E-6H-6, 19–50 cm. The shape of the C_{org} profile in Core UM26 is also included (for exact contents see Fig. 1). The shaded bands indicate the positions of the sapropels.

youngest sapropel. In addition, low-molecular-weight organic sulfur compounds are included in S_{elem}; these compounds may be significantly present in the sapropel in Section 969E-6H-6, 27 cm.

A remarkable feature is the enrichment of NaCl-extractable sulfur, probably gypsum (see following discussion), at the base of the sapropel in Section 969E-6H-6, 30 cm (Fig. 1). This presumed gypsum enrichment is associated with an enrichment of iron (hydr)oxides (Fe_{dith}, Fig. 3), indicating possible oxidation of iron sulfides within the sapropel layer. The oxidation is most likely the result of oxygen contamination during or after sampling. The iron sulfides prone to rapid oxidation are iron monosulfides. Gypsum may be

Table 2. Comparison between the total sulfur content of the sediments and S_{sum}.

Samples	Total sulfur (µmol/g dry)	S_{sum} (µmol/g dry)	Yield (%)
S1, UM26			
Above	56.6	46.4	82
Within	281.2	227.5	81
Below	256.1	178.1	70
160-967C-6H-2, 30 cm			
Above	53.7	49.9	93
Within	1079.1	986.1	91
Below	368.2	344.2	93
160-969E-6H-6, 27 cm			
Above	216.3	192.9	89
Within	1256.2	1164.3	93
Below	282.8	245.3	87

Notes: S_{sum} = the sum of the sulfur species measured in the sequential extraction, including residual S. The values are averages of samples grouped according to position relative to sapropel.

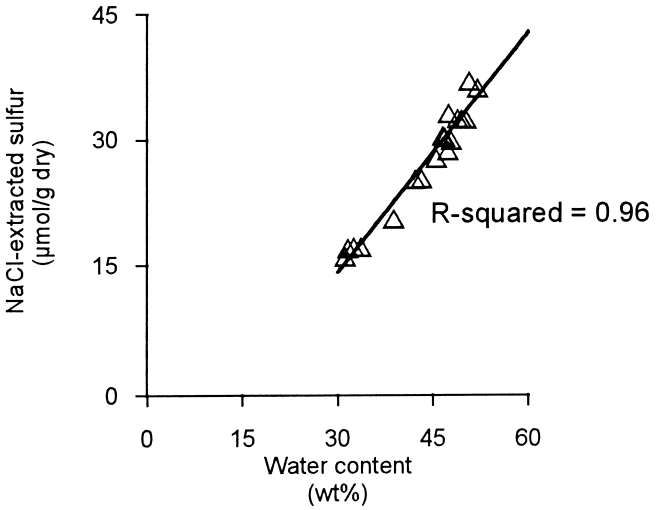

Figure 4. NaCl-extracted sulfur vs. water content in Core UM26.

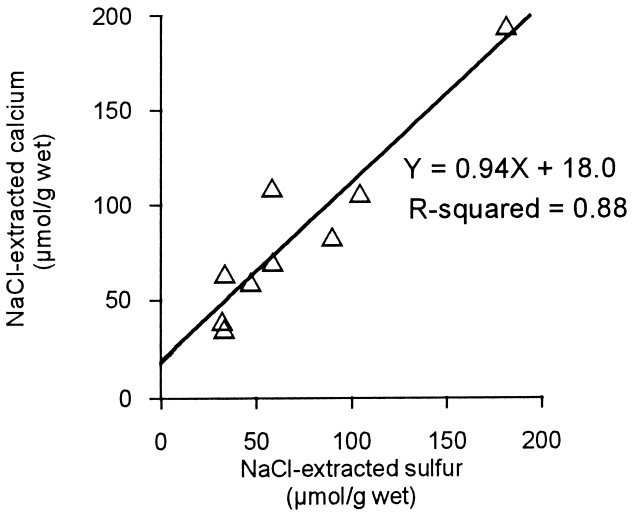

Figure 5. NaCl-extracted calcium vs. NaCl-extracted sulfur in interval 969E-6H-6, 19–50 cm.

formed as a consequence of oxidation of iron monosulfides (FeS_x, in which x is close to 1) and dissolution of carbonate tests, according to the following reaction:

$$4FeS_x + (3 + 6x)O_2 + (2 + 12x)H_2O + 8xCaCO_3 \rightarrow 4FeOOH + 4xCaSO_4 \cdot 2H_2O + 4xCa^{2+} + 8xHCO_3^-. \quad (1)$$

The ratio of iron (hydr)oxide to SO_4^{2-} in gypsum is $4:4x = 1:x$. Assuming that all SO_4^{2-} is extracted with NaCl, the 1:x ratio can be obtained from the ratio of excess dithionite-extracted iron to excess NaCl-extracted sulfur. The observed ratio is 1:1.07 (Fig. 6), which yields a mean formula for iron sulfide of $Fe_{0.93}S$. This corresponds to a mixture of mackinawite ($Fe_{0.995–1.023}S$, Ward, 1970) and greigite ($Fe_{0.75}S$), which is the most common association of iron monosulfide minerals found in sediments (Berner, 1967). Moreover, shipboard paleomagnetic measurements of three discrete samples taken immediately after core splitting from the base of the sapropel in Section 969E-6H-6, 27 cm, show a reduction in both magnetic remanence and susceptibility with time. The time-dependent decay in magnetic properties (10%/day) is consistent with oxidation of a metastable ferrimagnetic iron sulfide (Roberts et al., in press).

Oxidation of iron monosulfides results in the addition of Ca^{2+} and SO_4^{2-} to the sediment samples and interstitial waters. Ca^{2+} and SO_4^{2-}, which cannot have escaped by diffusion because the cores were sampled within a few hours after core splitting, and the samples are isolated in vials, will be extracted with NaCl. On the basis of reaction (1) one would expect to find a ratio of $\Delta Ca^{2+}:\Delta SO_4^{2-} = (4x + 4x):4x = 2:1$ in these NaCl extracts. Nonetheless, the amount of Ca^{2+} that dissolves will be controlled by the dynamic equilibria of the carbonate system and not just by the stoichiometry of reaction (1). Therefore, detailed mass balance calculations were performed. These calculations predict a linear correlation between Ca^{2+} and SO_4^{2-} in NaCl extracts with a slope of 1 (i.e., $\Delta Ca^{2+}:\Delta SO_4^{2-} = 1:1$; see Appendix). In fact, the correlation between Ca^{2+} and SO_4^{2-} in NaCl extracts of the sapropel in Section 969E-6H-6, 27 cm, has a slope of 0.94 (i.e., $\Delta Ca^{2+}:\Delta SO_4^{2-} \approx 1:1$; Fig. 5). Hence, the observed correlation between Ca^{2+} and SO_4^{2-} are most likely due to the oxidation of iron monosulfides.

Summarizing, the iron (hydr)oxide and S_{NaCl} enrichments at the base of the sapropel in Section 969E-6H-6, 27 cm, indicate the original presence of iron monosulfides ($FeS_{1.07}$, AVS). This appearance of AVS indicates that active SO_4^{2-} reduction may still occur within this sapropel. SO_4^{2-} reduction either never stopped inside this extremely C_{org}-rich layer or started again after some time. Assuming that porewater data for Hole 969A are comparable to those of Hole 969E, the porewater profile of SO_4^{2-} indicates that SO_4^{2-} reduction may only take place at very low rates (Emeis, Robertson, Richter, et al., 1996).

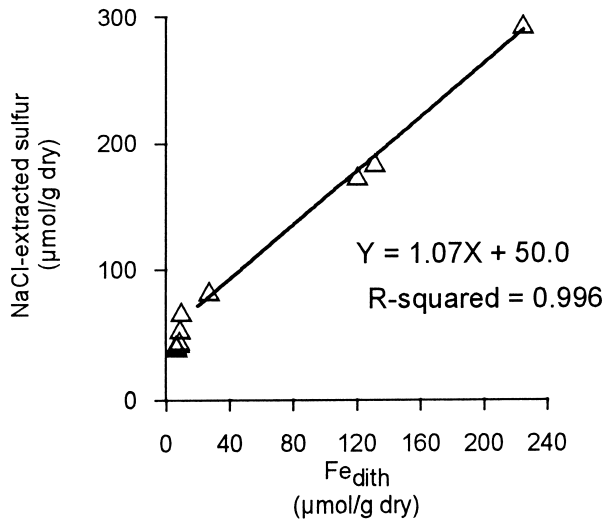

Figure 6. NaCl-extracted sulfur vs. Fe_{dith} (dithionite extracted iron) in interval 969E-6H-6, 19–50 cm.

Pyritic Sulfur, Humic Sulfur, and Nonextractable Organic Sulfur

Most of the sulfide that was formed in the sapropel and retained in the sediment has reacted with iron, and formed pyrite in and below the sapropel (Fig. 1), whereas another portion of the sulfide was incorporated in organic matter. The uptake of reduced sulfur in organic matter results in the fractions humic sulfur (S_{NaOH}, Fig. 1) and nonextractable organic sulfur (deduced from the residual fraction of the sequential extraction). Only in the central part of the sapropel in Section 969E-6H-6, 27 cm, nonextractable organic sulfur is detectable. In sediments with low reactive iron contents, reduced sulfur may be incorporated in the organic fraction of the sediments during early diagenesis (e.g., Sinninghe Damsté and De Leeuw, 1990).

The main sulfur compound below each sapropel is pyrite. The pyrite has been formed as a result of downward diffusion of HS^- from the sapropel during formation of the sapropel (Passier et al., 1996). Most of the sulfide that diffused to below the sapropel has reacted with iron (hydr)oxides in the underlying sediments or with upward-diffusing Fe^{2+}. Sediments below the sapropels, however, are also enriched in humic sulfur (S_{NaOH}, Fig. 1) as compared with sediments above the sapropels. This implies that the humic substances below the sapropels may have incorporated sulfur, during the downward diffusion of HS^-.

Storage of Reduced Sulfur and Iron

Carbon-Sulfur Relationships

The C_{org} content of the sapropels differs significantly. The 23.5 wt% C_{org} found in the sapropel in Section 969E-6H-6, 27 cm, is among the highest found in Eastern Mediterranean sediments (Emeis, Robertson, Richter, et al., 1996). The amount of reduced sulfur in sediments is closely related to the C_{org} content. This is due to the fact that with increasing amounts of C_{org} a larger amount of organic matter is metabolizable and more sulfide is produced (e.g., Berner and Raiswell, 1983; Berner, 1984; Leventhal, 1987). In normal marine sediments the relation between sulfur and carbon contents has a slope of 1/2.8 (S_{tot}/C_{org} ratio, wt%/wt%) and passes through the origin (assuming that sulfur fractions other than reduced sulfur are relatively negligible). In euxinic marine environments, however, sulfide is omnipresent (independent of local C_{org} contents) and iron sulfide formation can take place in the water column or at the sediment/water interface. In addition, even slowly reacting iron compounds may react with sulfide in euxinic environments. Consequently, positive intercepts on the sulfur axis are obtained in sulfur vs. carbon plots for euxinic sediments, and only weak correlations may be observed (e.g., Leventhal, 1983; Berner, 1984). Additionally, postdepositional sulfidization of C_{org}-poor sediments may result in extremely high sulfur/carbon ratios (Boesen and Postma, 1988; Middelburg, 1991; Leventhal, 1995; Passier et al., 1996).

In S_{tot} vs. C_{org} plots of the discussed sapropels (Fig. 7), most samples plot above the normal marine regression line, pointing to euxinic features and postdepositional sulfidization of C_{org}-poor sediments below the sapropels (Passier et al., 1996). The samples with extremely high C_{org} values from the sapropel in Section 969E-6H-6, 27 cm, however, plot below the normal marine line. Reduced sulfur formation and/or uptake in the sediment seems more limited for this part of the sapropel. There are several factors that determine the sulfur content of sediments in which sulfur is predominantly pyrite. Sulfate reduction and subsequent pyrite formation can be limited by (1) the

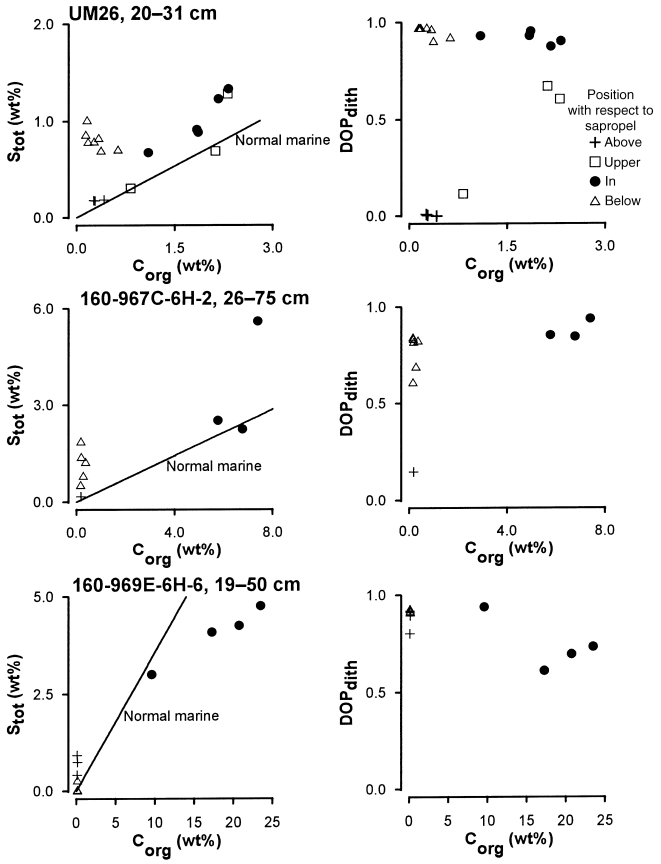

Figure 7. S_{tot} and DOP_{dith} vs. C_{org} in Core UM26, 20–31 cm, and intervals 967C-6H-2, 26–75 cm, and 969E-6H-6, 19–50 cm.

availability of SO_4^{2-}, (2) amount and reactivity of organic matter, and (3) content and reactivity of iron minerals (e.g., Berner, 1984).

Availability of Sulfate

The first factor, the availability of SO_4^{2-}, is neither the limiting factor in the marine environment where sapropels are formed nor in the present-day interstitial waters of the Eastern Mediterranean. Most of the porewater profiles of SO_4^{2-} in the Eastern Mediterranean demonstrate a downward increase owing to the dissolution of underlying evaporites, like the profiles at Sites 967 and 969 (Emeis, Robertson, Richter, et al., 1996). Preliminary sulfur isotope data and other sedimentary data show that the SO_4^{2-} concentration was not limiting for sulfide formation in the past either.

Reactivity of Organic Matter

The second factor, the availability of metabolizable organic matter, may be important in the sapropels. Apparently, the organic matter left over after intensive remineralization during and shortly after sapropel formation is no longer sufficiently labile to sustain a sulfate-reducing environment in most of the sapropels.

Furthermore, the relatively low sulfur content in the organic-rich samples of Section 969E-6H-6, 27 cm (Fig. 7), may be in part related to a lower reactivity of the organic matter. The humic sulfur and non-extractable organic sulfur contents in Section 969E-6H-6, 27 cm, are relatively high. Because of the incorporation of sulfur into organic substances, organic matter may become less labile (e.g., Sinninghe Damsté and De Leeuw, 1990). However, the C_{org} content is much higher in Section 969E-6H-6, 27 cm, than in Section 967C-6H-2, 30 cm, and Core UM26. Therefore, it seems unlikely that the uptake of sulfur into organic compounds has significantly affected the total reactivity of organic matter, and thus its reactivity for SO_4^{2-} reduction.

In summary, it seems that the reactivity of organic matter is presently limiting SO_4^{2-} reduction and pyrite formation in most sapropels, but the reason for this is not clear. The mechanisms that determined the extent of pyrite formation in each sapropel during the periods that SO_4^{2-} reduction was not limited by the reactivity of the organic matter are discussed subsequently.

Content and Reactivity of Iron Minerals

The third limiting factor for pyrite formation, the availability of iron, is usually inferred from plots of the degree of pyritization (DOP) vs. C_{org} (Raiswell and Berner, 1985). The parameter DOP was proposed by Berner (1970):

$$DOP = \frac{pyritic\ Fe}{pyritic\ Fe + reactive\ Fe}.$$

We have taken reactive iron as equal to dithionite-extractable iron, as recommended by Raiswell et al. (1994); DOP values based on dithionite-extractable iron are DOP_{dith} values.

The high DOP_{dith} values inside the sapropels, independent of C_{org} content, suggest that pyrite formation in the sapropels was iron limited (Fig. 7). However, as we explain later, the observed DOP_{dith} values indicate only that all iron that was supplied to the sediment was stored as pyrite.

Slightly lower DOP_{dith} values are found for the C_{org}-rich samples at the base of the sapropel in Section 969E-6H-6, 27 cm. These deviations are artificial, and they originate from the iron (hydr)oxide enrichment that formed as a result of iron sulfide oxidation, as discussed earlier (Fig. 3). If the oxidized sulfur had diffused out of the system, this would have evoked a deviation in the S_{tot} vs. C_{org} plot toward the C_{org} axis. Assuming that all oxidized sulfur has been retained in the sediment as gypsum, oxidation of iron sulfides does not influence the S_{tot} vs. C_{org} plot. Consequently, the relatively low sulfur/carbon ratios in the C_{org}-rich part of Section 969E-6H-6, 27 cm, cannot be explained by this oxidation.

High DOP_{dith} values and high sulfur/carbon ratios are acquired in C_{org}-poor sediments below the sapropels, as a result of postdepositional sulfidization (Fig. 7). This sulfidization developed as soon as the sulfide production exceeded the iron availability for pyrite formation in the sapropel (Passier et al., 1996). In Core UM26 and Section 967C-6H-2, 30 cm, this sulfidization has affected only the sediments underlying the sapropels and not the overlying sediments. This indicates that only small amounts of HS^- may have diffused out of the C_{org}-rich layers after sapropel formation. In Section 969E-6H-6, 27 cm, however, DOP_{dith} values and pyrite contents of the sediments overlying the sapropel are slightly higher than above the other sapropels (Fig. 7). Probably post- or syndepositional sulfidization of the sediments overlying the sapropel in Section 969E-6H-6, 27 cm, has occurred. At the moment it is not clear whether the sulfide source is upward sulfidization of the sapropel in Section 969E-6H-6, 27 cm, or downward HS^- diffusion from a younger sapropel.

Relatively low DOP_{dith} values at low C_{org}-contents are found above the sapropels in Core UM26 and Section 967C-6H-2, 30 cm. In the Eastern Mediterranean, sapropel formation is usually followed by a period of downward oxidation of the sediment. C_{org} and pyrite are oxidized at the oxidation front, and the front is marked by an iron (hydr)oxide enrichment (De Lange et al., 1989; Pruysers et al., 1993; Van Santvoort et al., 1996). Above the sapropels in Core UM26 and Section 967C-6H-2, 30 cm, such enrichments of iron (hydr)oxides are present (Fig. 3). The iron enrichment above sapropel S1 in Core UM26 indicates active oxidation of the sapropel (Van Santvoort et

al., 1996), whereas the iron enrichment above Section 967C-6H-2, 30 cm, is thought to be the relict of such a front. No iron (hydr)oxide enrichment is present above Section 969E-6H-6, 27 cm. Either an oxidation front has never been present above this sapropel or any oxidized iron has subsequently been reduced and diffused out of the sediment. It could have been used for pyrite formation elsewhere in the sediment or reacted to pyrite in situ. Accordingly, sediments above Section 969E-6H-6, 27 cm, do not have anomalously low DOP_{dith} values and the low DOP_{dith} values above the other two sapropels are caused by oxidation of pyrite and C_{org} and the precipitation of iron (hydr)oxides. The high-resolution samples from Core UM26 (Fig. 3) show that the iron (hydr)oxide-layer "invades" into the top of sapropel S1; this means that pyrite is more readily oxidized than C_{org}. Consequently, the sediments from this upper sapropel region have relatively low DOP_{dith} values at relatively high C_{org} contents. Although the oxidation of pyrite results in SO_4^{2-} formation (Moses et al., 1987), the oxidation at the oxidation front has not led to an enrichment of SO_4^{2-} (S_{NaCl}, Fig. 1) above the sapropels. This indicates that the oxidation is a slow process relative to diffusion of oxidized species away from the front.

The DOP_{dith} values lead to the conclusion that the availability of iron has been controlling the amount of pyrite stored within the sapropels. In the next section, we discuss the mechanisms that rule the storage of pyrite in the different sapropels in more detail.

Iron Source, Mobility, and Fixation

Iron Enrichments

Iron (hydr)oxides are not depleted in the sapropels relative to the underlying sediments (Fig. 3), although the sulfide concentration must have been higher inside the sapropels (sulfide source) than in the underlying sediments, where sulfide has diffused. In addition, DOP_{dith} values and (aluminum-normalized) silicate iron contents ($Fe_{silicate} = Fe_{tot} - Fe_{pyr} - Fe_{dith}$, and $Fe_{silicate}$* = average $Al_{tot} \times Fe_{silicate}/Al_{tot}$) within the sapropels are as high as those below the sapropels (Fig. 7; Table 3). This indicates that iron from slowly reacting iron-bearing silicates has not been detectably used as an extra source for pyrite formation inside the sapropel, where all reactive iron was incorporated in pyrite. If iron from silicates were used more extensively within sapropels, $Fe_{silicate}$ would have been lower and DOP_{dith} values would have been higher within the sapropel. The pyrite enrichments are not due to any sedimentary dilution effect, as follows from normalization to aluminum content (Fig. 3). As a consequence, because more pyrite has formed within than below the sapropels, there must have been an additional input of iron to the sapropel sediment.

Iron-C_{org} Relationships

In a plot of the sum of pyritic iron and dithionite-extractable iron vs. C_{org} in the sapropel samples, two groups of data points appear (Fig. 8). It is not important for the interpretation whether $Fe_{pyr} + Fe_{dith}$ or just Fe_{pyr} is used (Fig. 8). To study the limits of pyrite formation, we used a plot of Fe_{pyr} vs. C_{org} instead of S_{tot} vs. C_{org} because organic sulfur is also included in S_{tot}. The first group of data points is situated at relatively low C_{org} contents, including samples from Core UM26 and Section 967C-6H-2, 30 cm, and the second group at relatively high C_{org} contents represents Section 969E-6H-6, 27 cm (Fig. 8). Sedimentary dilution may be an important factor in the interpretation of enrichments in sediments. Therefore, the data were normalized with respect to Al_{tot}, assuming that aluminum fluxes to the sediment have remained constant. Plots of aluminum-normalized values of Fe_{pyr} (+ Fe_{dith}) vs. aluminum-normalized values of C_{org} yield the same general distinction between samples from Core UM 26 and Section 967C-6H-2, 30 cm, on one hand and samples from Section 969E-6H-6, 27 cm, on the other (Fig. 8). The uppermost sample, with the lowest C_{org} content, from the sapropel in Section 969E-6H-6, 27 cm, is separated from the C_{org}-rich samples of this sapropel, and plots in the same area as samples from Core UM26 and Section 967C-6H-2, 30 cm. For the first group a positive correlation between C_{org} contents and iron is discernible. The second group has a lower iron content, relative to C_{org}, and the iron content is independent of C_{org}.

Positive correlations between C_{org} and the sum of pyritic and reactive iron have been observed in previous studies of organic-rich sediments (Raiswell and Berner, 1985; Raiswell and Al-Biatty, 1989). This correlation may be either a diagenetic or a depositional feature.

The input of detrital iron to sediments may vary as a result of climate-related changes in weathering and erosion (Raiswell and Al-Biatty, 1989). However, the most extremely C_{org}-rich sapropel (Section 969E-6H-6, 27 cm), which is probably related to the most extreme climate changes, contains relatively little amounts of iron (Figs. 3, 8). Accordingly, an increase of detrital iron input does not

Table 3. Range of contents of $Fe_{silicate}$ and $Fe_{silicate}$*.

Samples	$Fe_{silicate}$ (mmol/g dry)	$Fe_{silicate}$* (mmol/g dry)
S1, UM26		
Within	247-265	255-265
Below	212-259	220-254
160-967C-6H-2, 30 cm		
Within	328-421	333-368
Below	229-456	281-698
160-969E-6H-6, 27 cm		
Within	107-379	158-543
Below	180-551	202-727

Notes: $Fe_{silicate} = Fe_{tot} - Fe_{pyr} - Fe_{dith}$. $Fe_{silicate}$* = average $Al_{tot} \times Fe_{silicate}/Al_{tot}$. The values are grouped according to position relative to sapropel.

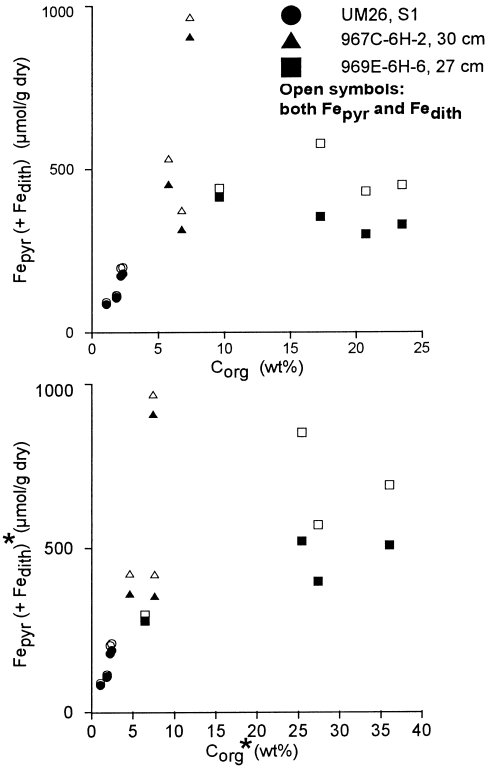

Figure 8. Fe_{pyr} (+Fe_{dith}) vs. C_{org} in sapropel samples from Core UM26, and intervals 967C-6H-2, 26–75 cm, and 969E-6H-6, 19–50 cm. $Fe_{pyr} = 0.5 \times S_{pyr}$, S_{pyr} is determined by Cr(II) reduction, and Fe_{dith} is dithionite-extractable iron. Asterisks indicate that the data have been normalized to aluminum content, for example: C_{org}* = average $Al_{tot} \times C_{org}/A_{ltot}$.

seem to be an important additional iron source during sapropel formation. Assuming that the input of detrital reactive iron is constant, there are two additional sources of iron during sapropel formation: (1) diffusion of Fe^{2+} from the underlying sediment to the sediment/water interface and (2) iron sulfide formation from dissolved Fe^{2+} and sulfide in the water column.

In these situations the supply of iron may be coupled to the C_{org} content via sulfide production. Positive iron vs. C_{org} correlations indicate that more SO_4^{2-} reduction has occurred and more pyrite has formed because more C_{org} is present. The mechanisms of pyrite enrichment and the correlation to the C_{org} content are discussed below.

Iron Addition via Diffusion from Underlying Sediments

A mechanism to explain the addition of iron and coupling between iron and C_{org} is that upward-diffusing Fe^{2+} is used for pyrite formation within the sapropel at times of relatively low sulfide production. Any diffusing Fe^{2+} that is not scavenged by pyrite formation in the sapropel may be oxidized near the sediment/water interface or may escape into the water column. In sediments with a higher C_{org} content, more metabolizable organic matter was originally present. Consequently, more SO_4^{2-} reduction and fixation of sulfide as pyrite was possible, leading to a positive correlation between Fe_{pyr} and C_{org}. In this situation, sulfide production, and thus indirectly the reactivity of organic matter toward SO_4^{2-} reduction determines the extent of pyrite formation, and sulfide consumes all available iron. The fixation of upward-diffusing Fe^{2+} as pyrite within the sapropel is possible only when the sulfide production is relatively small. When sulfide production is larger than the sum of the upward Fe^{2+} flux and detrital reactive iron input, sulfide will diffuse out of the sapropel and will meet upward-diffusing Fe^{2+} below it. Pyrite formation takes place below the sapropel, and the upward Fe^{2+} flux does not reach the sapropel. In that case, pyrite formation within the sapropel is limited by the amount of detrital reactive iron.

For sapropel S1, recent porewater fluxes of Fe^{2+} have been compared to the amount of iron fixed as pyrite within and below the sapropel (Passier et al., 1997). This comparison indicates that upward diffusion of Fe^{2+} during sapropel formation and detrital iron combined could have supplied all fixed iron. Similar calculations for older sapropels are difficult, because Fe^{2+} fluxes, detrital iron inputs, and duration of periods of sapropel formation are not known.

The amounts of iron fixed as pyrite in Sections 967C-6H-2, 30 cm, and 969E-6H-6, 27 cm, are higher than in Core UM26 (Fig. 8). Preliminary sulfur isotope measurements indicate that pyrite formation was probably not significant after burial of the sapropels. A similar conclusion was drawn for Pleistocene and Holocene sapropels (Passier et al., 1996, 1997). Hence, significant iron addition via diffusion from underlying sediments probably also stopped after burial, with the possible exception of the iron fixed as AVS and maybe some of the pyrite at the base of the sapropel in Section 969E-6H-6, 27 cm. The larger fixation of iron in Sections 967C-6H-2, 30 cm, and 969E-6H-6, 27 cm, compared with Core UM26 may also arise from a larger input of detrital reactive iron and/or a larger upward flux of Fe^{2+}. Within and below the sapropel in Section 967C-6H-2, 30 cm, Fe_{dith} is higher than within and below the other sapropels (Fig. 3). This site is close to Cyprus; consequently, the detrital input and flux of Fe^{2+} may have been larger here. However, there is no reason to assume a larger detrital iron input in Section 969E-6H-6, 27 cm, than in Core UM26, as the sites are close to each other. In addition, iron and C_{org} are not coupled in Section 969E-6H-6, 27 cm. Moreover, it was argued previously that the input of detrital iron did not increase significantly during sapropel formation. The scenario described here (i.e., pyrite enrichment via addition of upward-diffusing Fe^{2+}) may yield only an uncoupled iron and C_{org} situation in the sapropel when downward sulfidization occurs: in this case, detrital reactive iron is the only available iron for pyrite formation, and the absolute pyrite enrichment in this sapropel cannot be explained. Another mechanism of pyrite formation seems to be important in the sapropel in Section 969E-6H-6, 27 cm, which is discussed in the following section.

Iron Addition via Iron Sulfide Formation in the Water Column

Iron addition may also arise from the precipitation of iron sulfides in a euxinic water column. This mechanism was recently proposed for the Black Sea, where a large part of the water column contains sulfide and iron may be liberated from sediments in suboxic zones along the basin margins (Canfield et al., 1996). This process may result in the coupling of iron and C_{org}: the more C_{org} rains down, the more sulfide will be present in the water column, and the more iron sulfides can precipitate in the water column, thus inducing a positive correlation between C_{org} and Fe_{pyr} in the sediment. However, the water-column iron sulfide that is added to the sediments in euxinic basins is usually independent of the C_{org} content, because sulfide is omnipresent and not necessarily related to the local C_{org} content. In addition, the amount of iron sulfide that is formed in the water column may be limited by the thickness of the sulfidic layer in the water column (e.g., Leventhal, 1983, 1987). In the sapropel in Section 969E-6H-6, 27 cm, Fe_{pyr} ($+Fe_{dith}$) is higher within the sapropel than below the sapropel and independent of the C_{org} content (Fig. 8). Thus, addition of iron from the water column may have resulted in the relative pyrite enrichment inside the sapropel in Section 969E-6H-6, 27 cm. No coupling of iron and C_{org} is visible; so, no significant pyrite was formed from upward-diffusing Fe^{2+} in the sapropel. Apparently, upward-diffusing Fe^{2+} could not reach the sapropel because downward sulfidization occurred permanently during sapropel formation, implying a constantly high sulfide production. This observation is in agreement with the occurrence of iron sulfide formation in the water column, and the implicit presence of sulfide in the bottom water: when downward sulfide diffusion occurs out of a sapropel, sulfide is also expected to diffuse upward to the bottom water. Sulfide may be oxidized at the sediment/water interface or in the bottom water, but when the sulfide flux is relatively large, sulfidic bottom waters may develop. Furthermore, when downward sulfidization takes place, pyrite formation within the sapropel is iron limited and uptake of sulfur in organic substances may be important (e.g., Sinninghe Damsté and De Leeuw, 1990). Hence, the presence of high amounts of organic sulfur in Section 969E-6H-6, 27 cm, can be explained.

Consequences of the Imbalance Between Sulfide Production and the Addition of Iron

In summary, in these sediments with predominantly syngenetic pyrite, the absence or presence of a positive correlation between Fe_{pyr} ($+Fe_{dith}$) and C_{org} may indicate the site of pyrite formation: in the water column (absence of correlation) or at the sediment/water interface (positive correlation).

Because mechanisms such as sulfidization of adjacent sediments and iron addition to the sediments are possible in the alternating C_{org}-rich and C_{org}-poor sediments in the Eastern Mediterranean, the site of SO_4^{2-} reduction does not necessarily coincide with the location of pyrite formation. Although iron sulfide formation may be (temporarily) limited within a sapropel, sulfide production within this layer may result in the formation of iron sulfides in the water column or below the sapropel. As the sulfidization of organic-poor sediments below sapropels invokes high sulfur/carbon ratios, the sediments from where the sulfur originates will have lower sulfur/carbon ratios when sulfide diffuses out of the source sediment (sapropel). Downward sulfidization has been important during the formation of the sapropel in Section 969E-6H-6, 27 cm, as a result of the extremely high C_{org} content. This may explain the apparent sulfur deficiency in these sediments (Fig. 7). In contrast, as long as downward sulfidization does not occur, the supply of Fe^{2+} to the sapropel results in a higher fixation capacity for sulfide within the sapropels, and thus in higher S_{tot} contents. This is expressed by the fact that many sapropel samples lie

far above the normal marine regression line in S_{tot} vs. C_{org} plots (e.g., Section 967C-6H-2, 30 cm, and Core UM26; Fig. 7).

CONCLUSIONS

The elevated C_{org} contents of sapropels have induced anoxic, sulfate-reducing sedimentary conditions and the fixation of reduced sulfur. Pyrite is the main sulfur species in the sediments in and below the sapropels. The presence of AVS in the extremely organic-rich (up to 23.5%) sapropel in Section 969E-6H-6, 27 cm, indicates that detectable, but slow, sulfate reduction still occurs in that interval.

Two postdepositional changes are important in the cyclic sediments in the Eastern Mediterranean: (1) sulfidization of sapropel-underlying sediments during sapropel formation, and (2) oxidation of sapropel and overlying sediments after sapropel burial. The sulfidization results in elevated pyrite contents, and, to a lesser extent, in elevated humic sulfur contents below each sapropel. Furthermore, sulfidization of the sediments both underlying and overlying a sapropel may happen around extremely organic-rich sapropels, where sulfate reduction continues after sapropel formation.

The iron sources for pyrite formation may comprise (1) Fe^{2+} diffusing upward from underlying sediments, (2) detrital iron, and (3) water-column iron through iron sulfide formation in the water column. Syngenetic pyrite formation during sapropel development takes place at the sediment/water interface or in the water column. Water-column iron sulfide formation has probably been important in the most organic-rich (up to 23.5%) sapropel (in Section 969E-6H-6, 27 cm), implying that the bottom waters contained sulfide during a substantial part of the formation of this sapropel. During the formation of sapropels with lower C_{org} contents, iron sulfide formation in the water column, and thus sulfidic bottom waters, were probably not as important.

Addition of iron to the site of sulfide production, the sapropel, results in higher sulfur fixation relative to the C_{org} content in sapropels, whereas downward sulfidization results in a lower fixation of sulfur relative to C_{org} content within the sapropels. Although sulfur fixation is enhanced below a sapropel, sulfur may also escape upward into the bottom water during periods of downward sulfidization. This escaped reduced sulfur may either oxidize at the chemocline or form iron sulfide in the water column.

The enrichment of Fe_{pyr} in the sediments is controlled primarily by the amount of iron that is added to the sediment interval and fixed by direct iron sulfide formation, rather than by the amount of detrital Fe: when more iron is added by diffusion from underlying sediments or by precipitation of iron sulfides in the water column, more pyrite is found in the sediments. The extent of the Fe_{pyr} enrichment within sapropels depends on the relative magnitudes of the sulfide production in the sapropel and the addition of iron to the sapropel during its formation.

ACKNOWLEDGMENTS

P.R. van der Linde (Geochemistry, Utrecht University) is gratefully acknowledged for doing the equilibrium calculations on the oxidation of sulfides, presented in the Appendix. M.E. Böttcher (ICBM, Oldenburg University) is thanked for the preliminary sulfur isotope measurements. Chief scientist C. Corselli, NIOZ technicians, and Captain Lubrano and his crew are thanked for their cooperation during the cruise with *Urania*. H.C. de Waard, D. van der Meent, R. Alink, G.N. Nobbe, and P.G.J. Anten provided valuable assistance in the lab. C.H. van der Weijden is thanked for critically reading the manuscript. The journal reviewers K. Wallman and M.E. Böttcher, as well as editor K.-C. Emeis are thanked for their constructive comments. This study was supported by the Netherlands Organization of Scientific Research (NWO/GOA, in particular GJdL by grant #750.00.620-7290), the MAST-2 *Palaeoflux* programme (#MAS2-CT93-0051), and the Cosiglio Nazionale della Ricerche (CNR). This is publication #970131 of the Netherlands Research School of Sedimentary Geology.

REFERENCES

Berner, R.A., 1967. Thermodynamic stability of sedimentary iron sulphides. *Am. J. Sci*., 265:777–785.

————, 1970. Sedimentary pyrite formation. *Am. J. Sci.*, 268:1–23.

————, 1984. Sedimentary pyrite formation: an update. *Geochim. Cosmochim. Acta,* 48:605–615.

Berner, R.A., and Raiswell, R., 1983. Burial of organic carbon and pyrite sulfur in sediments over Phanerozoic time: a new theory. *Geochim. Cosmochim. Acta,* 47:855–862.

Boesen, C., and Postma, D., 1988. Pyrite formation in anoxic environments in the Baltic. *Am. J. Sci*., 288:575–603.

Calvert, S.E, and Karlin, R.E., 1991. Relationships between sulphur, organic carbon, and iron in modern sediments of the Black Sea. *Geochim. Cosmochim. Acta,* 55:2483–2490.

Canfield, D.E., 1989. Sulfate reduction and oxic respiration in marine sediments: implications for organic carbon preservation in euxinic environments. *Deep-Sea Res. Part A,* 36:121–138.

Canfield, D.E., Lyons, T.W., and Raiswell, R., 1996. A model for iron deposition to euxinic Black Sea sediments. *Am. J. Sci.,* 296:818–834.

Canfield, D.E., Raiswell, R., Westrich, J.T., Reeves, C.M., and Berner, R.A., 1986. The use of chromium reduction in the analysis of reduced inorganic sulfur in sediments and shale. *Chem. Geol.*, 54:149–155.

Cutter, G.A., and Oatts, T.J., 1987. Determination of dissolved sulfide and sedimentary sulfur speciation using gas chromatography photoionization detection. *Anal. Chem.*, 59:717–721.

de Lange, G.J., Middelburg, J.J., and Pruysers, P.A., 1989. Discussion: Middle and Late Quaternary depositional sequences and cycles in the Eastern Mediterranean. *Sedimentology,* 36:151–158.

Emeis, K.-C., Robertson, A.H.F., Richter, C., et al., 1996. *Proc. ODP, Init. Repts.*, 160: College Station, TX (Ocean Drilling Program).

Ferdelman, T., Church, T.M., and Luther, G.W., III, 1991. Sulfur enrichment of humic substances in a Delaware salt marsh sediment core. *Geochim. Cosmochim. Acta,* 55:979–988.

Francois, R., 1987. A study of the extraction conditions of sedimentary humic acids to estimate their true in situ sulfur content. *Limnol. Oceanogr.*, 32:964–972.

Froelich, P.N., Klinkhammer, G.P., Bender, M.L., Luedtke, N.A., Heath, G.R., Cullen, D., Dauphin, P., Hammond, D., Hartman, B., and Maynard, V., 1979. Early oxidation of organic matter in pelagic sediments of the eastern equatorial Atlantic: suboxic diagenesis. *Geochim. Cosmochim. Acta,* 43:1075–1090.

Henneke, E., 1993. Early diagenetic processes and sulfur speciation in pore waters and sediments of the hypersaline Tyro and Bannock Basins, eastern Mediterranean [Ph.D. thesis]. Utrecht Univ., *Geol. Ultraiectina,* 108.

Henneke, E., Luther, G.W., III, De Lange, G.J., and Hoefs, J., 1997. Sulphur speciation in anoxic hypersaline sediments from the Eastern Mediterranean Sea. *Geochim. Cosmochim. Acta,* 61:307–321.

Higgs, N.C., Thomson, J., Wilson, T.R.S., and Croudace, I.W., 1994. Modification and complete removal of eastern Mediterranean sapropels by postdepositional oxidation. *Geology,* 22:423–426.

Köster, H.M., 1979. *Die chemische Silikatanalyse:* Berlin (Springer-Verlag).

Kostka, J.E., and Luther, G.W., III, 1994. Partitioning and speciation of solid phase iron in saltmarsh sediments. *Geochim. Cosmochim. Acta,* 58:1701–1710.

Leventhal, J.S., 1983. An interpretation of carbon and sulfur relationships in Black Sea sediments as indicators of environments of deposition. *Geochim. Cosmochim. Acta,* 47:133–137.

————, 1987. Carbon and sulfur relationships in Devonian shales from the Appalachian Basin as an indicator of environment of deposition. *Am. J. Sci.*, 287:33–49.

————, 1995. Carbon-sulfur plots to show diagenetic and epigenetic sulfidation in sediments. *Geochim. Cosmochim. Acta,* 59:1207–1212.

Luther, G.W., III, and Church, T.M., 1992. An overview of the environmental chemistry of sulfur in wetland systems. *In* Howarth, R.W., Stewart, J.W.B., and Ivanov, M.V. (Eds.), *Sulfur Cycling on the Continents:* New York (John Wiley and Sons), 125–142.

Middelburg, J.J., 1991. Organic carbon, sulphur, and iron in Recent semi-euxinic sediments of Kau Bay, Indonesia. *Geochim. Cosmochim. Acta,* 55:815–828.
Morel, F.M.W., and Hering, J.G., 1993. *Principles and Applications of Aquatic Chemistry:* New York (Wiley).
Moses, C.O., Nordstrom, D.K., Herman, J.S., and Mills, A.L., 1987. Aqueous pyrite oxidation by dissolved oxygen and by ferric iron. *Geochim. Cosmochim. Acta,* 51:1561–1571.
Mossmann, J.R., Aplin, A.C., Curtis, C.D., and Coleman, M.L., 1991. Geochemistry of inorganic and organic sulphur in organic-rich sediments from the Peru Margin. *Geochim. Cosmochim. Acta,* 55:3581–3595.
Passier, H.F., Middelburg, J.J., de Lange, G.J., and Böttcher, M.E., 1997. Pyrite contents, microtextures and sulphur isotopes in relation to formation of the youngest Eastern Mediterranean sapropel. *Geology,* 25:519–522.
Passier, H.F., Middelburg, J.J., Van Os, B.J.H., and De Lange, G.J., 1996. Diagenetic pyritization under Eastern Mediterranean sapropels caused by downward sulphide diffusion. *Geochim. Cosmochim. Acta,* 60:751–763.
Pruysers, P.A., de Lange, G.J., Middelburg, J.J., and Hydes, D.J., 1993. The diagenetic formation of metal-rich layers in sapropel-containing sediments in the eastern Mediterranean. *Geochim. Cosmochim. Acta,* 57:527–536.
Raiswell, R., and Al-Biatty, H.J., 1989. Depositional and diagenetic C-S-Fe signatures in early Paleozoic normal marine shales. *Geochim. Cosmochim. Acta,* 53:1147–1152.
Raiswell, R., and Berner, R.A., 1985. Pyrite formation in euxinic and semi-euxinic sediments. *Am. J. Sci.,* 285:710–724.
Raiswell, R., Canfield, D.E., and Berner, R.A., 1994. A comparison of iron extraction methods for the determination of degree of pyritisation and the recognition of iron-limited pyrite formation. *Chem. Geol.,* 111:101–110.
Roberts, A.P., Stoner, J.S., and Richter, C., in press. Diagenetic magnetic enhancement of sapropels from the eastern Mediterranean Sea. *Mar. Geol.*
Sinninghe Damsté, J.S., and De Leeuw, J.W., 1990. Analysis, structure and geochemical significance of organically-bound sulfur in the geosphere: state of the art and future research. *Org. Geochem.,* 16:1077–1101.
Van Os, B.J.H., Middelburg, J.J., and de Lange, G.J., 1991. Possible diagenetic mobilisation of barium in sapropelic sediment from the Eastern Mediterranean. *Mar. Geol.,* 100:125–136.
Van Santvoort, P.J.M., de Lange, G.J., Thomson, J., Cussen, H., Wilson, T.R.S., Krom, M.D., and Ströhle, K., 1996. Active post-depositional oxidation of the most recent sapropel (S1) in sediments of the Eastern Mediterranean. *Geochim. Cosmochim. Acta.,* 60:4007–4024.
Ward, J.C., 1970. The structure and properties of some iron sulfides. *Rev. Pure Appl. Chem.,* 20:175–206.
Whitfield, M., 1974. The ion-association model and the buffer capacity of the carbon dioxide system in seawater at 25 °C and 1 atmosphere total pressure. *Limnol. Oceanol.,* 19:235–248.
Zhabina, N.N., and Volkov, I.I., 1978. A method of determination of various sulfur compounds in sea sediments and rocks. *In* Krumbein, W.E. (Ed.), *Environmental Biogeochemistry and Geomicrobiology* (Vol. 3): Ann Arbor (Ann Arbor Sci. Publ.), 735–746.

Date of initial receipt: 6 January 1997
Date of acceptance: 6 June 1997
Ms 160SR-020

APPENDIX

Oxidation of sedimentary FeS_x, in which x is close to one, and consequent changes in Ca, SO_4, and Fe chemistry were modeled. The net oxidation reaction is

$$4FeS_x + (3 + 6x)O_2 + (2 + 4x)H_2O \rightarrow 4FeOOH + 8 \times H^+ + 4 \times SO_4^{2-} \quad . \qquad (A1)$$

Reaction (A1) corresponds to the formation of sulfuric acid in the calcareous sediment.

As a result, carbonate dissolves, and Ca^{2+} is liberated. The addition of sulfuric acid to the sediment can be modeled as the addition of an amount of acid to a calcite suspension, using the basic interpretation of the alkalinity as a balance of charges (e.g., Morel and Hering, 1993):

$$\text{Alk} = \text{excess negative charge from weak acids} = \text{excess positive charge from strong base}, \qquad (A2)$$

we obtain:

$$Alk = [OH^-] - [H^+] + [HCO_3^-] + 2[CO_3^{2-}] + \ldots = [Na^+] + [K^+] + 2[Ca^{2+}] + 2[Mg^{2+}] - [Cl^-] - 2[SO_4^{2-}] + \ldots \qquad (A3)$$

In the "acid-addition" experiment, all terms om the right-hand side, except $[Ca^{2+}]$ and $[SO_4^{2-}]$, are constant. Consequently,

$$[Ca^{2+}] = [SO_4^{2-}] + \tfrac{1}{2} \times ([OH^-] - [H^+] + [HCO_3^-] + 2[CO_3^{2-}]) + \textit{constant}. \qquad (A4)$$

Even when we use the exact definition of alkalinity (e.g., Morel and Hering, 1993) and take into account the formation of carbonate complexes, which comprise about 35% of the total dissolved carbonate in seawater (e.g., $NaCO_3^-$ and $CaCO_3^0$), the same equation (i.e., A4) is obtained.

According to Equation A4, $[Ca^{2+}] : [SO_4^{2-}] = 1:1$, on the condition that the second term on the right-hand side ("TERM," half the alkalinity, neglecting carbonate complexes) is relatively constant.

To study the response of this term to the addition of sulfuric acid, chemical equilibrium calculations on a simple model system were done. This model system closely resembles the sedimentary situation at Hole 969A at 51.34 mbsf from which pore waters were analyzed (Emeis, Robertson, Richter, et al., 1996). This sedimentary environment is assumed to be present in the sapropel in Section 160-969E-6H-6, 27 cm, before FeS_x is oxidized. This model system consists of an inert electrolyte at 0.72 M, 31.8-mM sulfate, 38.7-mM acid, and calcite (solid); from this system 18.9-mM CO_2 has been withdrawn; the temperature is 25°C and the pressure is 1 atm. In this system equilibrium with atmospheric CO_2 is not taken into account, because the pore waters were analyzed and sediment samples were stored in closed vials only a few hours after core splitting, whereas the CO_2 gas-solution equilibration times are in the order of days (FeS_x oxidation takes place between core splitting and storage). The vials have minimal headspace; therefore, equilibrium with CO_2 (gas) can be neglected as well. For this system, neglecting the formation of complexes, the following values were calculated: $[Ca^{2+}]$ = 19.7-mM, $[SO_4^{2-}]$ = 31.8-mM, and $[OH^-] - [H^+] + [HCO_3^-] + 2[CO_3^{2-}]$ = 0.760-mM. The shipboard measurements of these parameters at 51.34 mbsf in Hole 969A are $[Ca^{2+}]$ = 21.7-mM, $[SO_4^{2-}]$ = 31.8-mM, and alkalinity = 1.882-meq/L (Emeis, Robertson, Richter, et al., 1996). Regarding the fact that in seawater about 90% of Ca is present as free Ca^{2+} and the $([OH^-] - [H^+] + [HCO_3^-] + 2[CO_3^{2-}])$ contributes approximately 65% of the alkalinity (Whitfield, 1974), this model can be considered reasonable for the sediment samples before oxidation.

The addition of sulfuric acid, representing the oxidation of FeS_x, to the initial system described previously was modeled. The variation in the second term on the right-hand of Equation A4 ("TERM"), as a function of the total sulfate concentration (which is proportional to the amount of acid added), is given in Figure A1. Compared to the changes in $[Ca^{2+}]$ and $[SO_4^{2-}]$, this term appears to be practically constant, resulting in a linear relationship, with a slope of 1, between $[SO_4^{2-}]$ ($[H_2SO_4]_{added}$) and $[Ca^{2+}]$ (Fig. A1). In these calculations it was assumed that CO_2 (gas), possibly evolved during oxidation, was conserved in the system. However, when the loss of CO_2(gas), which occurs during transfer of the sample to an N_2 atmosphere, is included in the calculations, the linear relationship between $[Ca^{2+}]$ and $[SO_4^{2-}]$ is maintained.

The pH variation is also shown in Figure A1. Because the pH decreases to below the pK_a value (6.15 for seawater) of the H_2CO_3/HCO_3^- equilibrium, the linear correlation between $[Ca^{2+}]$ and $[SO_4^{2-}]$ can easily be seen when reaction (1) (see "Discussion" section) is rewritten with H_2CO_3 as the principal component, rather than HCO_3^-.

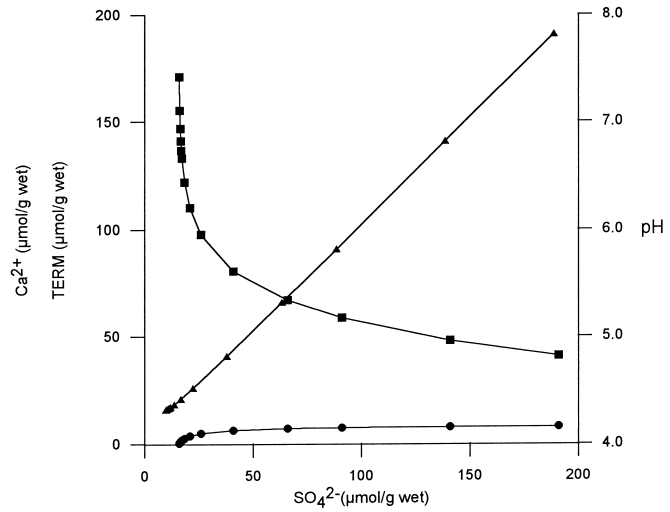

Figure A1. The calculated values of $\frac{1}{2} \times ([OH^-] - [H^+] + [HCO_3^-] + 2[CO_3^{2-}])$ ("TERM," circles), $[Ca^{2+}]$ (triangles), and pH (squares) as a function of the total concentration of SO_4^{2-} (initial $[SO_4^{2-}]$ + added sulfuric acid). The data are expressed in contents in wet sediment (µmol/g wet), enabling direct comparison to the data depicted in Figure 5. A water content of 50% is assumed (y mM = $0.5 \times y$ µmol/g wet).